DOI: 10.1002/chem.200801369

A Synthetic, Structural, Spectroscopic and DFT study of Re^{I}, Cu^{I}, Ru^{II} and Ir^{III} Complexes Containing Functionalised Dipyrido[3,2-*a*:2′,3′-*c*]phenazine (dppz)

Natasha J. Lundin,[b] Penny J. Walsh,[a] Sarah L. Howell,[a] Allan G. Blackman,[a] and Keith C. Gordon*[a]

Abstract: The ligands 11-cyanodipyrido[3,2-*a*:2′,3′-*c*]phenazine and 2-(11-dipyrido[3,2-*a*:2′,3′-*c*]phenazine)-5-phenyl-1,3,4-oxadiazole have been coordinated to Re^{I}, Cu^{I}, Ru^{II} and Ir^{III} metal centres. Single-crystal X-ray analyses were performed on *fac*-chlorotricarbonyl(11-cyanodipyrido[3,2-*a*:2′,3′-*c*]phenazine)rhenium ($C_{22}H_9ClN_5O_3Re$, $a=6.509(5)$, $b=12.403(5)$, $c=13.907(5)$ Å, $\alpha=96.88(5)$, $\beta=92.41(5)$, $\gamma=92.13(5)°$, triclinic, $P\bar{1}$, $Z=2$) and bis-2,2′-bipyridyl(2-(11-dipyrido[3,2-*a*:2′,3′-*c*]phenazine)-5-phenyl-1,3,4-oxadiazole)ruthenium triflate·2 CH_3CN ($C_{52}H_{36}F_6N_{12}O_8RuS_2$, $a=10.601(5)$, $b=12.420(5)$, $c=20.066(5)$ Å, $\alpha=92.846(5)$, $\beta=96.493(5)$, $\gamma=103.720(5)°$, triclinic, $P\bar{1}$, $Z=2$). The ground- and excited-state properties of the ligands and complexes have been investigated with a range of techniques, including electrochemistry, absorption and emission spectroscopy, spectroelectrochemistry and excited-state lifetime studies. Spectroscopic, time-resolved and DFT studies reveal that the ligand-centred (LC) transitions and their resultant excited states play an important role in the photophysical properties of the complexes. Evidence for the presence of lower-lying metal-to-ligand charge-transfer transitions is obtained from resonance Raman spectroscopy, but nanosecond transient Raman experiments suggest that once excited, the ^{3}LC state is populated.

Keywords: density functional calculations · dipyridophenazine · electronic structure · ligand effects · N heterocycles

Introduction

The development of energy-efficient goods and processes is becoming progressively more important as the demand for electrical energy increases. The production of lighting sources which are bright, portable, flexible and above all energy-efficient is a goal that may be fulfilled by the continued development of organic light-emitting diodes (OLEDs).[1–3] OLEDs are multi-layer thin-film devices that can efficiently convert electrical energy into light.[4,5] OLEDs do this by allowing holes and electrons to be transported from opposing electrodes through charge-transporting materials via the highest occupied molecular orbitals (HOMOs) and lowest unoccupied molecular orbitals (LUMOs), respectively. The charges then recombine in an emissive material to form an exciton, or excited state, the relaxation of which can result in light emission.[6] The emission properties of OLEDs are determined by the compounds present in the layers, as well as layer homogeneity and thickness, so control over device properties may, in principle, be readily achieved.

The energies of the charge-carrying molecular orbitals in OLEDs have certain requirements. The E_{HOMO} needs to increase on moving spatially from the anode to the emitting layer for effective hole transport. In the case of electron transfer from the cathode to the emitting layer, the LUMOs are involved in sequential electron-transfer reactions in which the E_{LUMO} decreases to facilitate electron transfer. As a result the relative band gap and absolute HOMO and LUMO energies of materials in OLEDs are of crucial importance to their efficiency and brightness. Balanced transport of electrons and holes is also required.[3] To fulfil these

[a] Dr. P. J. Walsh, Dr. S. L. Howell, Prof. A. G. Blackman, Prof. K. C. Gordon
Department of Chemistry, University of Otago
Union Place, PO Box 56, Dunedin (New Zealand)
Fax: (+64) 3-479-7906
E-mail: kgordon@chemistry.otago.ac.nz

[b] Dr. N. J. Lundin
School of Chemistry, University of Dublin
Trinity College, Dublin 2 (Ireland)

Supporting information for this article is available on the WWW under http://dx.doi.org/10.1002/chem.200801369.

 © 2008 Wiley-VCH Verlag GmbH & Co. KGaA, Weinheim WILEY InterScience DISCOVER SOMETHING GREAT

energetic requirements, OLEDs typically contain a number of layers of different compounds between the electrodes.

The choice of emissive dopant in an OLED therefore plays a large role in the brightness, colour, efficiency and lifetime of the device. Herein, the syntheses of some emissive dyes based on the polypyridyl ligand dipyrido[3,2-*a*:2′,3′-*c*]phenazine (dppz), which have potential for incorporation into OLEDs, are reported and their properties investigated. Complexes of dppz have been examined extensively with respect to their ability to behave as "molecular light switches" for DNA in aqueous solution. Complex cations, such as $[Ru(bpy)_2(dppz)]^{2+}$ and $[Ru(dppz)(phen)_2]^{2+}$ (bpy: 2,2′-bipyridine, phen: 1,10-phenanthroline), show minimal emission in aqueous solution but intense emission if DNA is introduced.[7–9] In aqueous solution, emission from the complex is negligible, because water interacts with the phenazine (phz)-type nitrogen atoms of dppz, thereby providing a low-energy non-radiative decay pathway.[10,11] If these nitrogen atoms cannot engage in hydrogen bonding, through either the presence of a non-polar solvent or addition of DNA to the aqueous solution, then intense, long-lived emission from the complex is observed. DNA is able to protect the phz-type nitrogen atoms from hydrogen bonding by allowing intercalation of the complex into its double helix.[8,12,13]

The unusual electronic structure of dppz has inspired numerous studies of both the ligand and its transition-metal complexes. Dppz may be thought of as comprising two components: a phen unit and a phz unit.[14] These two subunits behave essentially separately, with many molecular orbitals (MOs) being localised over only one subunit. Of particular importance are the three lowest-lying unoccupied MOs; those labelled $4a_2$ and $5b_1$(phen) are localised on the phen region, whereas $4b_1$(phz) is contained in the phz region (Figure 1).[15–17] Although the b_1(phz) MO is the lowest in

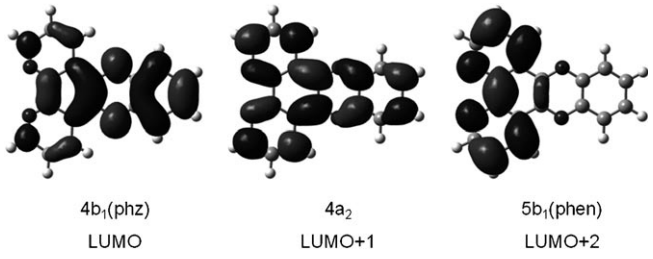

Figure 1. Molecular orbital diagrams for the three LUMOs of dppz.

energy for dppz, the similarity in the energies of these orbitals means that their ordering may be altered by chelation of a metal centre at N4 and N5 or by substitution of the ligand. This can affect the nature of the lowest-energy excited state in complexes of dppz and its derivatives.

Herein, we describe the synthesis and characterisation of dppz ligands substituted at the 11-position with either a nitrile or 5-phenyl-1,3,4-oxadiazole group (Scheme 1), and Re^{I}, Ru^{II}, Cu^{I} and Ir^{III} complexes of these ligands. The

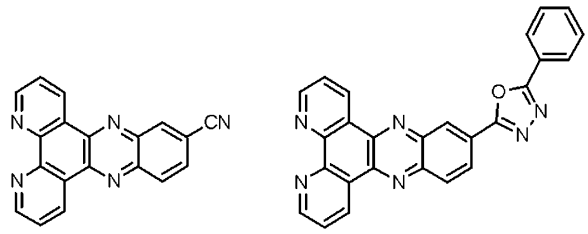

Scheme 1. Structures of the ligands investigated. Right: 11-cyanodipyrido[3,2-*a*:2′,3′-*c*]phenazine; left: 2-(11-dipyrido[3,2-*a*:2′,3′-*c*]phenazine)-5-phenyl-1,3,4-oxadiazole.

ground- and excited-state properties were investigated by a variety of spectroscopic (UV/Vis, resonance and transient Raman and photoluminescence) and other methods (crystallography, electrochemistry and spectroelectrochemistry) in concert with density functional theory (DFT) calculations. The crystal structures of *fac*-chlorotricarbonyl(11-cyanodipyrido[3,2-*a*:2′,3′-*c*]phenazine)rhenium ([Re(dppzCN)$(CO)_3$Cl]) and bis-2,2′-bipyridyl(2-(11-dipyrido[3,2-*a*:2′,3′-*c*]phenazine)-5-phenyl-1,3,4-oxadiazole)ruthenium triflate ($[Ru(bpy)_2(dppzoxad)](CF_3SO_3)_2{\cdot}2\,MeCN{\cdot}H_2O$) are presented.

Results and Discussion

Structural studies: Crystallographic data for [Re(dppzCN)$(CO)_3$Cl] and $[Ru(bpy)_2(dppzoxad)](CF_3SO_3)_2{\cdot}2\,MeCN{\cdot}H_2O$ are presented in Table 1 and ORTEP diagrams of the complexes are given in Figure 2 and Figure 3, respectively. Selected bond lengths and angles are also presented in Tables 2 and 3. The Re^{I} centre of [Re-

Table 1. Crystallographic data for [Re(dppzCN)$(CO)_3$Cl] and $[Ru(bpy)_2(dppzoxad)](CF_3SO_3)_2{\cdot}2\,MeCN{\cdot}H_2O$.

	[Re(dppzCN)$(CO)_3$Cl]	$[Ru(bpy)_2(dppzoxad)](CF_3SO_3)_2{\cdot}2\,MeCN{\cdot}H_2O$
formula	$C_{22}H_9ClN_5O_3Re$	$C_{52}H_{36}F_6N_{12}O_8RuS_2$
formula weight	612.99	1236.12
space group	$P\bar{1}$	$P\bar{1}$
Z	2	2
crystal system	triclinic	triclinic
a [Å]	6.5085(2)	10.6005(7)
b [Å]	12.4030(3)	12.4204(9)
c [Å]	13.9072(4)	20.0661(13)
α [°]	96.880(1)	92.846(3)
β [°]	92.408(1)	96.493(4)
γ [°]	92.132(1)	103.720(3)
V [Å^3]	1112.58(5)	2542.1(17)
ρ_{calcd} [Mg m^{-3}]	1.615	1.830
T [K]	85(2)	85(2)
λ [Å]	0.71073	0.71073
μ [mm^{-1}]	5.614	0.482
$R1$[a]	0.0269	0.0522
$wR2$[b]	0.0700	0.1458

[a] Conventional R on F_{hkl}: $\Sigma||F_o|-|F_c||/\Sigma|F_o|$. [b] Weighted R on $|F_{hkl}|^2$: $\{\Sigma[w(F_o^2-F_c^2)^2]/\Sigma[w(F_o^2)^2]\}^{1/2}$.

 © 2008 Wiley-VCH Verlag GmbH & Co. KGaA, Weinheim

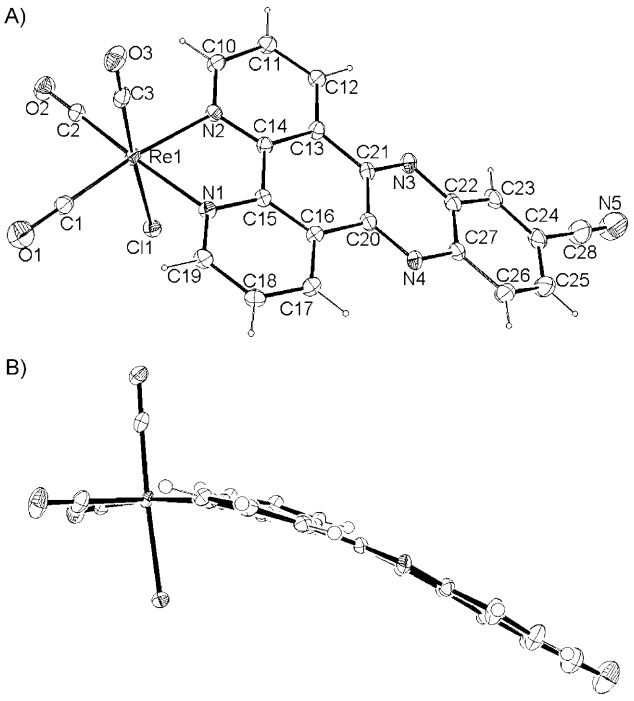

Figure 2. A) ORTEP diagram of [Re(dppzCN)(CO)$_3$Cl] showing the numbering scheme. B) Side view emphasising the curvature of the dppz ligand.

Table 2. Selected bond lengths [Å] and angles [°] for [Re(dppzCN)(CO)$_3$Cl].

Re1−N1	2.179(3)	Re1−C1	1.924(4)
Re1−N2	2.176(3)	Re1−C2	1.924(3)
Re1−Cl1	2.4834(8)	Re1−C3	1.897(4)
N1-Re1-N2	75.35(10)	N2-Re1-C3	93.89(12)
N1-Re1-Cl1	81.93(7)	Cl1-Re1-C1	92.87(11)
N1-Re1-C1	99.23(13)	Cl1-Re1-C2	91.14(10)
N1-Re1-C2	170.95(12)	Cl1-Re1-C3	176.98(10)
N1-Re1-C3	95.93(12)	C1-Re1-C2	86.86(15)
N2-Re1-Cl1	83.51(7)	C1-Re1-C3	89.58(15)
N2-Re1-C1	173.82(12)	C2-Re1-C3	90.76(14)
N2-Re1-C2	98.18(12)		

Table 3. Selected bond lengths [Å] and angles [°] for the [Ru(bpy)$_2$(dppzoxad)]$^{2+}$ ion.

Ru1−N1	2.062(4)	Ru1−N4	2.070(4)
Ru1−N2	2.066(4)	Ru1−N5	2.061(4)
Ru1−N3	2.050(4)	Ru1−N6	2.069(4)
N1-Ru1-N2	91.53(14)	N2-Ru1-N6	94.37(16)
N1-Ru1-N3	93.57(14)	N3-Ru1-N4	89.59(15)
N1-Ru1-N4	174.28(15)	N3-Ru1-N5	98.02(16)
N1-Ru1-N5	95.49(15)	N3-Ru1-N6	169.69(15)
N1-Ru1-N6	79.15(14)	N4-Ru1-N5	79.32(16)
N2-Ru1-N3	78.41(15)	N4-Ru1-N6	98.30(15)
N2-Ru1-N4	93.78(15)	N5-Ru1-N6	90.00(16)
N2-Ru1-N5	172.32(15)		

(dppzCN)(CO)$_3$Cl] is in a distorted octahedral environment due to the small bite angle of dppzCN of 75.35°. The Ru^{II} metal centre in the crystal structure of [Ru(bpy)$_2$(dppzoxad)]$^{2+}$ also displays a distorted octahedral geometry. The three bidentate ligands are unable to accommodate bite angles of 90°, and display N-Ru-N angles of 78.42 and 79.32° for the two bpy ligands and 79.15° for the Ru^{II} metal centre.[18–21]

The dppzCN ligand in [Re(dppzCN)(CO)$_3$Cl] shows pronounced non-planarity, as can be seen in Figure 2. We have previously observed similar behaviour in related complexes[22] but the effect is more pronounced in this case. To quantify the extent of deviation from planarity, we calculated the mean deviation of the ligand atoms (excluding hydrogen atoms) from the plane defined by the two coordinating N atoms (N1 and N2 in this case) and the metal ion for this, and a number of other complexes containing dppz or its derivatives.[21–26] These data, which are given in Table 4, show that [Re(dppzCN)(CO)$_3$Cl] exhibits the largest overall deviation from planarity of all the complexes considered.

As has been suggested for distorted dppz backbones in other complexes,[22] the curvature observed for [Re(dppzCN)(CO)$_3$Cl] may be caused by a combination of crystal packing effects and disruption of π–π stacking interactions between the dppz ligands (Figure 4A). [Re(dppzCN)(CO)$_3$Cl] shows some offset face-to-face π–π stacking interactions between the aromatic rings of the dppz framework; however, these are greatly decreased in number compared to the crystal structure of dppz itself,[27] and the presence of a metal centre and nitrile substituent appears to impede the formation of the face-to-face arrangement that the free dppz ligand adopts. The crystal structure of [Ru(bpy)$_2$(dppzoxad)]-(CF_3SO_3)$_2$·2MeCN·H_2O shows a number of offset face-to-face π–π stacking interactions between the dppz-based ligands (Figure 4B) that lie within the usual range for these interactions.[28] The aromatic 1,3,4-oxa-

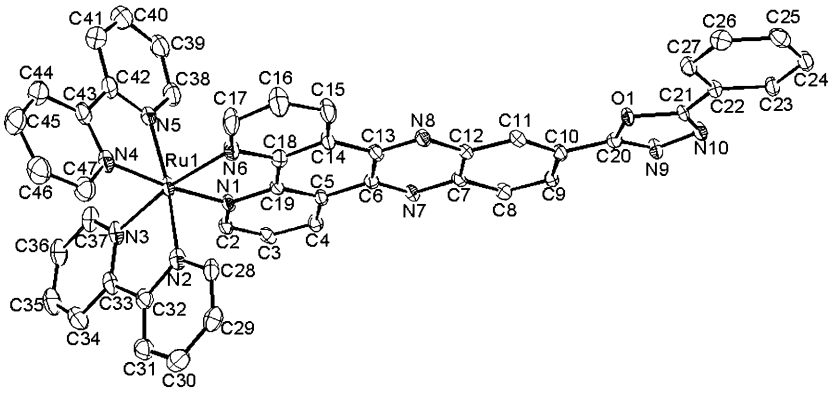

Figure 3. ORTEP diagram of the [Ru(bpy)$_2$(dppzoxad)]$^{2+}$ ion.

 © 2008 Wiley-VCH Verlag GmbH & Co. KGaA, Weinheim

Table 4. Deviations of atoms in the dppz ligand from the N-M-N plane in a range of complexes.

Compound	Mean deviation [Å]	Largest deviation [Å]
$[Re(dppzCN)(CO)_3Cl]$	1.033	3.140
$[Ru(bpy)_2(dppzoxad)]^{2+}$	0.375	1.146
$[Re(dppzCOOEt)(CO)_3Cl]$[a]	0.559	1.631
$[Re(dppzBr)(CO)_3Cl]$[a]	0.491	1.454
$[Re(dppz)(4\text{-mepy})(CO)_3]CF_3SO_3$[b]	0.190	0.573
$[Re(bdppz)(4\text{-mepy})(CO)_3]CF_3SO_3$[c]	0.051	0.197
[Cu(dppz){tris(3-phenylpyrazolyl)-borate}](ClO_4)[d]	0.509	1.413
$[Pt(dppz)Cl_2]$[e]	0.041	0.139
$[Ru(bpy)_2(dndz)](PF_6)_2$[f]	0.418	1.334

[a] From Lundin et al.;[22] dppzCOOEt: dipyrido[3,2-*a*:2′,3′-*c*]phenazine-11-carboxylic ethyl ester, dppzBr: 11-bromodipyrido[3,2-*a*:2′,3′-*c*]phenazine. [b] From Yam et al.;[25] 4-mepy: 4-methylpyridine. [c] From Yam et al.;[26] bdppz: benzodipyrido[3,2-*a*:2′,3′-*c*]phenazine. [d] From Dhar et al.[23] [e] From Kato et al.[24] [f] From Rusanova et al.;[21] dndz: 11,12-dicyanodipyrido[3,2-*a*:2′,3′-*c*]phenazine.

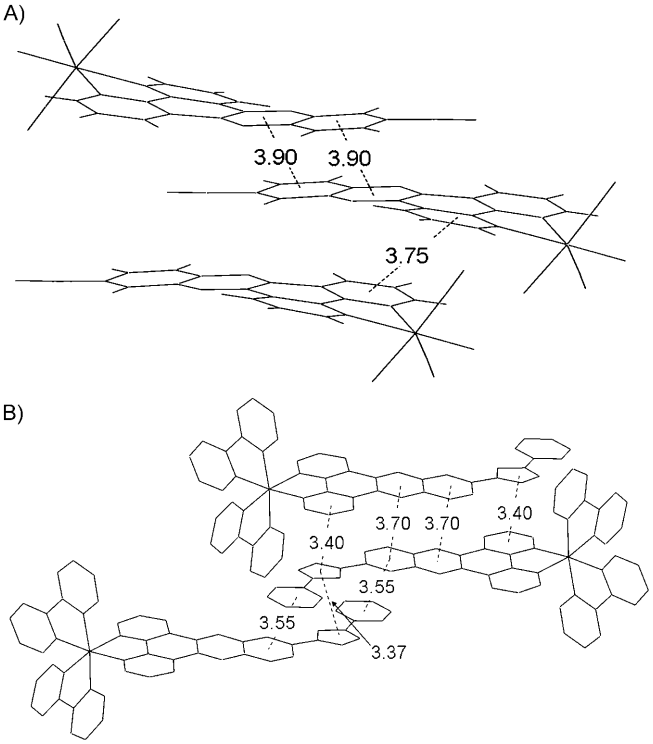

Figure 4. π–π stacking interactions of aromatic rings in A) [Re(dppzCN)(CO)$_3$Cl] and B) $[Ru(bpy)_2(dppzoxad)]^{2+}$ showing centroid–centroid distances between closest rings [Å].

diazole substituent is involved in these interactions, which presumably contribute to the observed planarity of the dppz backbone in the crystal structure of this complex.

The structure of [Re(dppzCN)(CO)$_3$Cl], as determined from DFT calculations, shows an average bond-length deviation of 0.2 pm when compared to the crystallographic data. The bending of the ligand seen in the crystal structure is not observed in the calculated structure. However, the ligand is predicted to lie at an angle to the equatorial plane; the mean plane of the pyrazine ring in the ligand (C20, C21, N3, C22, C27, N4) forms an angle of 17° with the plane defined by the Re and *trans*-CO ligands (Re1, C1, C2); in the crystal structure this deviation is 31°. The analogous inter-plane angle for the related complex [Re(dppzCOOEt)(CO)$_3$Cl] is experimentally 17° and calculated as 15°. Hence the bending of the ligand that is evident in Figure 2 may be due to strong intermolecular forces.

Electronic structure: DFT calculations (B3LYP) indicate that the CN and oxadiazole substituents affect the energy of the 4b$_1$(phz)-based LUMO (Figure 5). It is also possible to

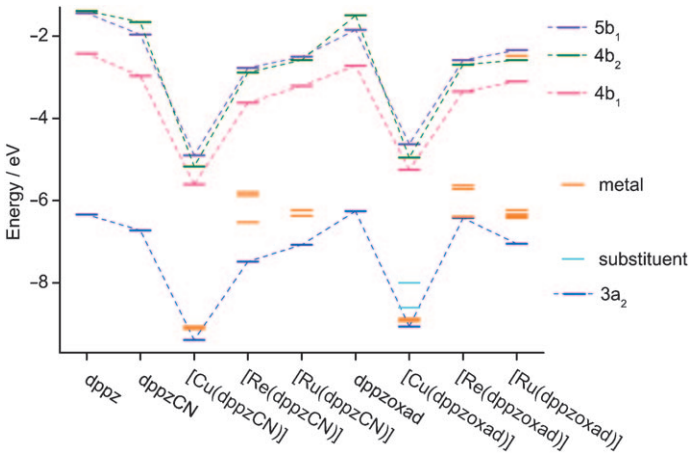

Figure 5. Energy levels of MOs across the series.

model the effect of metal coordination and results show that this stabilises the 5b$_1$ MO. Some care is required in making such comparisons, particularly for the Ru complexes. For $[Ru(dppz)(phen)_2]^{2+}$, DFT calculations in vacuo predict the HOMO to be dppz-based—this is clearly incorrect, as shown by the experimental optical and electrochemical properties.[29] This may be corrected by the inclusion of solvent effects[29] which result in a reordering of the MOs, with the t$_{2g}$(Ru) being the HOMO. Geometry optimisation that includes solvation effects on molecules of this size can be problematic and an alternative, less computationally intensive approach is to optimise in vacuo and then perform a single-point energy calculation with solvent included. This approach has been successfully applied to $[Ru(dppz)(phen)_2]^{2+}$.[29] We used a similar approach for both $[Ru(bpy)_2(dppzCN)]^{2+}$ and $[Ru(bpy)_2(dppzoxad)]^{2+}$. This results in HOMOs that are t$_{2g}$(Ru) orbitals. Control calculations on the free ligand reveal negligible reordering. The Re and Cu complexes show metal-based orbitals as HOMOs for in vacuo calculations. A comparison of in vacuo and solvent-included single-point energy calculations for the Re complexes shows there is little effect on MO energy reordering, although the absolute energies are greatly altered.[30]

Absorption spectroscopy: Absorption data for the complexes are presented in Table 5. The spectra of dppzoxad

 © 2008 Wiley-VCH Verlag GmbH & Co. KGaA, Weinheim

Table 5. Absorption data for ligands and complexes

Compound	Wavelength [nm] ($\varepsilon \times 10^{-4}$ L mol^{-1} cm^{-1})
dppz[a]	270 (6.07), 295 (sh)[b], 315 (sh), 343 (0.75), 351 (0.86), 360 (1.19), 367 (1.05), 378 (1.29)
dppzoxad[c]	276 (4.07), 349 (0.72), 367 (0.95), 376 (sh), 385 (1.10), 400 (0.88)
[Re(dppzoxad)(CO)$_3$Cl][c]	288 (sh), 301 (3.51), 350 (sh), 389 (1.43), 403 (1.37)
dppzCN	271 (2.28), 351 (sh), 357 (sh), 367 (0.63), 376 (sh), 388 (0.67)
[Re(dppzCN)(CO)$_3$Cl]	279 (6.60), 320 (1.29), 364 (1.14), 393 (sh)
[Cu(dppzCN)(PPh$_3$)$_2$]$^+$	274 (9.89), 349 (sh), 364 (1.73), 377 (1.67)
[Cu(dppzoxad)(PPh$_3$)$_2$]$^+$	266 (3.14), 272 (3.14), 299 (sh), 382 (0.73), 398 (0.77)
[Ru(bpy)$_2$(dppzCN)]$^{2+}$	279 (21.9), 315 (sh), 347 (sh), 356 (3.60), 363 (3.76), 373 (3.74), 439 (3.12)
[Ru(bpy)$_2$(dppzoxad)]$^{2+}$	287 (21.8), 314 (sh), 377 (5.60), 393 (6.23), 440 (3.79)
[Ir(dppzCN)(ppy)$_2$]$^+$	278 (10.46), 333 (sh), 370 (1.87), 394 (sh), 475 (0.12)
[Ir(dppzoxad)(ppy)$_2$]$^+$	270 (5.75), 286 (sh), 301 (5.43), 389 (2.05), 410 (2.09), 470 (0.09)

[a] As reported by Amouyal et al.[43] [b] sh: shoulder. [c] As previously reported.[44]

and dppzCN are typical for dppz-based compounds,[14,31] with a higher-energy transition assigned as ligand centred (LC) $\pi\rightarrow\pi^*$ in nature and a number of lower-energy bands that are attributed to $\pi\rightarrow\pi^*$ or $n\rightarrow\pi^*$ transitions. Absorption maxima for all of the compounds occur at a slightly lower energy than for dppz itself; this is consistent with the LUMOs of the ligands being lowered in energy by the presence of an electron-withdrawing substituent. The shift of absorption bands with substitution at the 11-position of dppz suggests that, as for dppz, the LUMOs of these ligands are located over the phz region of the molecule. In the spectra of the complexes the highest-energy LC transition shifts to a slightly longer wavelength compared with the free ligands, which is consistent with the LUMOs being further lowered in energy upon coordination. The only exceptions are [Cu(dppzoxad)(PPh$_3$)$_2$]$^+$ and [Ir(dppzoxad)(ppy)$_2$]$^+$, which show a slight blue shift and a broadening and splitting of the higher-energy transitions. Metal-to-ligand charge-transfer (MLCT) transitions appear as lower-energy shoulders on the LC bands for the Re^{I}, Cu^{I} and Ir^{III} complexes. The Ru^{II} complexes display a characteristic lower-energy MLCT transition, which occurs between a metal-based dπ MO and the b$_1$(phen)-based MO of dppz.[17]

Resonance Raman spectra: It is possible to gain insight into the nature of electronic transitions by using resonance Raman spectroscopy.[32] Raman transitions that are strongly enhanced are those that mimic the structural distortion present with photoexcitation to the excited state.[33,34] Thus, if the vibrational modes are known then the strongly enhanced bands can provide some insight into the nature of the electronic transition.[35] For a meaningful interpretation of such data to be made, the vibrational modes of the compound of interest must be calculated correctly. We use the mean absolute deviation between experimental and predicted frequencies to parameterise the effectiveness of the calculations.[36] The vibrational modes are available from those analyses.

It should be possible to ascertain the MO populated in the Franck–Condon (FC) state from the pattern of band enhancements in the resonance Raman spectra. For the complexes with only one polypyridyl ligand (the Cu and Re complexes), there are two types of transitions that can contribute to the absorption spectra of the complexes in the low-energy region: the MLCT and LC transitions.[37] In *fac*-[Re(dppz)(CO)$_3$Cl] there is a prevalence of enhanced modes which are phen-based.[16] For this complex the FC state is Re$\rightarrow$[b$_1$(phen)]. For the complex *fac*-[Re(dppz)(py)(CO)$_3$]$^+$, the "precursor" state formed is a LC state, possibly π–π^* (phen).[38] We have recently shown that an analysis of the frontier MOs with the resonance Raman intensity patterns may be used to infer the accepting orbital in an MLCT transition.[39]

The resonance Raman spectra of the ligands generated with 356 nm excitation provide a signature for the ^{1}LC transitions. For dppzoxad there are significant differences between the normal and resonance spectra. The resonance spectrum is dominated by a band at 1540 cm^{-1} which is barely visible in the normal spectrum. Furthermore, the strong normal Raman bands at 1628, 1609, 1587 and 1561 cm^{-1} are very weak in the resonance spectrum. The vibrational analysis reveals that the strongly enhanced bands are due to phz (1441 cm^{-1}), delocalised (1470 cm^{-1}) and oxadiazole (1540 cm^{-1}) vibrations. This finding is consistent with the resonant transition being HOMO$\rightarrow$LUMO (Figure 6), as both of these orbitals have significant phz and oxadiazole character with less amplitude on the phen portion of the ligand. By comparing the resonance Raman spectra of the complexes to those of the ligand it is possible to detect other transitions that may be present at 356 nm. For [Cu(dppzoxad)(PPh$_3$)$_2$]$^+$ and [Re(dppzoxad)(CO)$_3$Cl] the spectra are very similar to that of the ligand, which indicates that at this wavelength, the ^{1}LC transition is the dominant chromophore. The presence of a band at 1449 cm^{-1} in the spectra of the complexes may suggest some MLCT character at this wavelength. This mode is associated with a delocalised vibration with phen character. However, this must be a relatively weak transition as the CO bands of the Re complex are not evident.[39] In the case of the Ru complex,

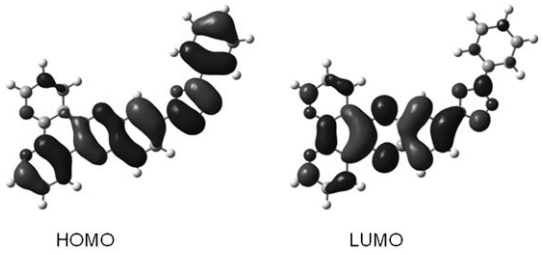

Figure 6. Diagrams of the HOMO and LUMO of dppzoxad.

 © 2008 Wiley-VCH Verlag GmbH & Co. KGaA, Weinheim

the Ru→bpy MLCT transitions also show resonance at 356 nm. The resonance Raman spectrum of [Re(dppzoxad)$(CO)_3$Cl] at 413 nm reveals the presence of an MLCT transition with strong enhancement of the CO band at 2029 cm^{-1}; the pattern of ligand band enhancements is consistent with population of a LUMO that has phen character, as the phen-based vibrations at 1632, 1610, 1563 and 1450 cm^{-1} are enhanced. The phz-based mode at 1419 cm^{-1} shows significantly less intensity, as do the other ^{1}LC marker bands. These data indicate that the ^{1}LC transitions have the same orbital character for the ligand and the Re and Cu complexes. An important result from these findings is that they suggest that the presence of the 11-position substituents does not lead to a significant breakdown in the dppz-like electronic character; that is, distinct phen- and phz-based MOs still exist.

Electrochemistry: Electrochemical data for the compounds are presented in Table 6. HOMO and LUMO energy levels have been calculated from the data by using previously described methods.[40] The nitrile and 5-phenyl-1,3,4-oxadiazole substituents at the 11-position result in dppzCN and dppzoxad being reduced at less negative potentials than dppz. This in turn lowers the LUMO energy levels of these ligands, which should make them better electron-transport agents than dppz. The influence of the substituent at the 11-position on the reduction potential suggests that the "redox" MO is at least partially located over the phz region of the ligand. The ligands display no reversible oxidation processes within the dichloromethane solvent window. Coordination of the ligands to a metal centre further lowers the LUMO energy levels, which should result in the complexes being even better electron-transport agents than the ligands, as the complexes are reduced at a less negative potential than the ligands.[14] The first reduction potentials for all of the complexes are consistent with the LUMOs of all of the complexes being phz-based. The extent of the lowering of the reduction potential upon coordination to a metal centre varies between 0.16 and 0.28 V. The first oxidation potentials of the complexes are attributed to oxidation of the metal centres. For the Re^I complexes, this is irreversible and appears at nearly as high a positive potential as for the free ligands. The Ru^{II} complexes possess a reversible oxidation at low positive potential, so correspondingly have the highest HOMO energy level which should make them the best hole-transport agents in an OLED. Reversible oxidations were observed at around +1.4 V versus SCE for all of the Ir^{III} complexes. This finding has been attributed to the Ir^{IV}/Ir^{III} redox couple, as for other similar Ir^{III} complexes.[41,42]

Table 6. Electrochemical data for ligands and complexes.

Compound	E_{ox}[a] [V]	E_{red}[a] [V]	$E_{(HOMO)}$[b] [eV]	$E_{(LUMO)}$[b] [eV]
dppz		−1.30[c]	−6.22[d]	−2.96[d]
dppzoxad[e]	1.69[f]	−0.85	−5.87	−3.31
[Re(dppzoxad)$(CO)_3$Cl][e]	1.62[f]	−0.75	−5.79	−3.36
dppzCN	1.83[f]	−0.91	−5.99	−3.25
[Re(dppzCN)$(CO)_3$Cl]	1.76[f]	−0.63	−5.92	−3.53
[Cu(dppzCN)$(PPh_3)_2$]$^+$	1.54	−0.68	−5.7	−3.48
[Cu(dppzoxad)$(PPh_3)_2$]$^+$	1.48	−0.78	−5.64	−3.38
[Ru(bpy)$_2$(dppzCN)]$^{2+}$	1.24	−0.75	−5.4	−3.41
[Ru(bpy)$_2$(dppzoxad)]$^{2+}$	1.2	−0.7	−5.36	−3.46
[Ir(dppzCN)$(ppy)_2$]$^+$	1.44	−0.64	−5.6	−3.52
[Ir(dppzoxad)$(ppy)_2$]$^+$	1.43	−0.74	−5.59	−3.42

[a] Redox potentials are reported versus SCE. [b] HOMO and LUMO energy levels were calculated by the method of Li et al.[40] [c] From Fees et al.[14] and converted to versus SCE from versus Fc^+/Fc (Fc: ferrocene) by adding 0.31 V to all potentials.[45] [d] From David et al.[46] [e] As previously reported; included for comparison.[44] [f] Oxidation potential is irreversible.

Spectroelectrochemical studies: Spectroelectrochemical studies were performed for all of the ligands and complexes. Difference spectra (Figure 7) were calculated by subtracting an initial spectrum of each material with no applied potential from spectra obtained at a large enough applied potential to induce a change from the ground state. The spectroelectrochemical results for dppzCN closely resemble those observed for dppz.[17] Peaks present in the neutral species decrease in intensity upon ligand reduction. New peaks appear at 340 and 530 nm. The broad band centred around 530 nm is attributed to a LC π→π* transition, as found previously for dppz.[14] The behaviour is consistent with the accepted electron being localised on the phz region of dppzCN. Different behaviour was observed for dppzoxad, with a general increase in absorption intensity. This may be caused by passivation of the ligand to the working electrode surface, an effect that has been observed for the closely related ligand ppb.[20] If this is occurring, then these spectra for dppzoxad cannot be considered representative of the reduced ligand.

The complexes [Re(dppzoxad)$(CO)_3$Cl], [Re(dppzCN)$(CO)_3$Cl], [Ru(bpy)$_2$(dppzCN)]$^{2+}$, [Ru(bpy)$_2$(dppzoxad)]$^{2+}$,[Ir(dppzCN)$(ppy)_2$]$^+$ and [Ir(dppzoxad)$(ppy)_2$]$^{2+}$ behaved in a similar manner to dppz. The spectroelectrochemical results for all of these complexes imply that an electron is added preferentially to the b_1(phz) MO of the dppz-based ligand, thus suggesting that the LUMO is phz-based.

Atypical spectroelectrochemical behaviour was observed for the Cu^I complexes [Cu(dppzCN)$(PPh_3)_2$]$^+$ and [Cu(dppzoxad)$(PPh_3)_2$]$^+$, both of which show a blue shift of the intense LC band at 280 nm. This behaviour suggests that the ligands may be dissociating from the Cu^I centre so that the absorption spectra of the free ligands are increasingly observed. It is well known that Cu^I complexes permit ligand exchange and speciation is often difficult to control, particularly for sterically demanding ligands.[47–49] Although the dppz-based ligands are not considered sterically demanding and so are not expected to encourage ligand lability, application of a negative potential may provide enough driving force to cause ligand dissociation from the Cu^I centre; this is not without precedent.[50]

Calculations on the reduced complexes of dppzCN reveal notable lengthening (C21–N3, N3–C22, C23–C24, N4–C20)

 © 2008 Wiley-VCH Verlag GmbH & Co. KGaA, Weinheim

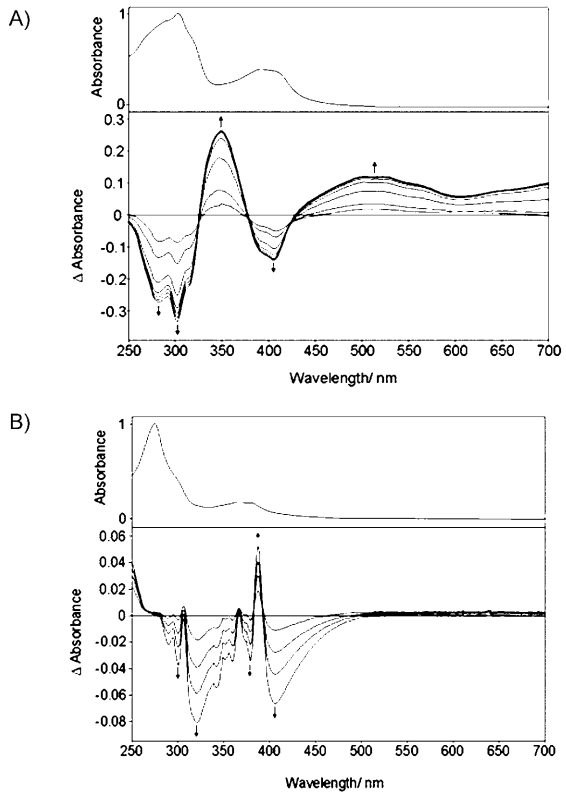

Figure 7. Difference spectra obtained from spectroelectrochemical studies of A) $[Re(dppzoxad)(CO)_3Cl]^{0/-}$ and B) $[Cu(dppzCN)(PPh_3)_2]^{+/0}$. The absorption spectrum of the neutral compound is shown above in each case for clarity.

and shortening (C15–C14, C25–C28; as labelled in Figure 2) of the bonds in the phz ring, consistent with the population of a phz-based MO. For the dppzoxad complexes the situation is less clear cut; $[Cu(dppzoxad)(PPh_3)_2]^0$ and $[Re(dppzCN)(CO)_3Cl]^-$ exhibit similar amounts of structural distortion of the dppzoxad ligand (the sum of absolute bond length changes being approximately 0.3 Å) consistent with phz MO population, but the distortion is much less for $[Ru(bpy)_2(dppzoxad)]^+$. The singly occupied MO (SOMO) calculated for these compounds reflects this in that the $[Ru(bpy)_2(dppzoxad)]^+$ has significant amplitude on the ancillary bpy ligands, whereas the SOMOs for $[Cu(dppzoxad)(PPh_3)_2]^0$ and $[Re(dppzCN)(CO)_3Cl]^-$ are phz-based.

It is possible to use resonance Raman spectroelectrochemistry to investigate the reduced species. However, only $[Re(dppzCN)(CO)_3Cl]$ provides a useful spectrum of the reduced species as, for other compounds, emission obscured the Raman data. Prior to reduction, no spectrum is observed from the parent species because it does not appreciably absorb at the excitation wavelength (514.5 nm). Upon the application of a reducing potential the sample solution darkens and the resonance Raman spectrum of $[Re(dppzCN)(CO)_3Cl]^-$ may be observed. This shows strong features at 1593 and 1587 cm^{-1} with weaker bands at 1562, 1515 and 1270 cm^{-1}. The strong bands correspond to the phen (at 1579 cm^{-1}) and phz (1571 cm^{-1}) modes, respectively. The similar modes in the parent species are observed (and predicted) at 1606 (1601) and 1549 (1547) cm^{-1}. The spectroelectrochemistry thus points to structural changes at the phz portion of the ligand, consistent with the calculations.

Excited-state studies: OLEDs operate through electron-induced emission, so the solution-based photoluminescence (PL) properties of a compound provide an approximation of the possible solid-state electroluminescence behaviour.[51] PL data for the compounds are presented in Table 7. The ligands display fluorescence, with the aromatic 5-phenyl-1,3,4-oxadiazole substituent of dppzoxad improving its quantum yield over that of dppzCN, due to the extended conjugation and increased rigidity of dppzoxad. The ligands exhibit long lifetimes consistent with ^{3}LC decay. The complexes are all emissive to some degree, with a mixture of states contributing to the observed profiles. Emission maxima for the complexes span a wide range of wavelengths due to the different metal centres affecting the relative input of LC and MLCT states. The Re^I complexes $[Re(dppzoxad)(CO)_3Cl]$ and $[Re(dppzCN)(CO)_3Cl]$ exhibit very weak, short-lived emission, consistent with efficient non-radiative decay from a ^{3}MLCT excited state, similar to the emission observed for other Re^I complexes containing dppz-based ligands with electron-withdrawing substituents. Very weak, short-lived emission from $[Cu(dppzCN)(PPh_3)_2]^+$ appears to occur from a mixture of ^{3}LC and ^{3}MLCT states.[31] This seems feasible, as other similar compounds are known to emit from more than one excited state at room temperature.[52] PL from $[Cu(dppzoxad)(PPh_3)_2]^+$ is consistent with ligand-based fluorescence (^{1}LC) as the emission appears at a very similar wavelength to that for uncoordinated dppzoxad, exhibits band structure and shows a significantly higher quantum yield than [Cu-

Table 7. Photoluminescence data for the compounds.

Compound	λ_{PL}[a] [nm]	Φ_{PL}[b]	Stokes shift[c] [cm^{-1}]	τ[d] [μs]
dppzoxad[e]	427	0.04	1600	10.6
$[Re(dppzoxad)(CO)_3Cl]$[e]	497	0.001	2600	<0.02
dppzCN	438	0.002	2700	6.6
$[Re(dppzCN)(CO)_3Cl]$	493	2.4×10^{-4}	5100	$\ll0.02$[f]
$[Cu(dppzCN)(PPh_3)_2]^+$	476, 600	8.6×10^{-5}	5500	<0.02[g]
$[Cu(dppzoxad)(PPh_3)_2]^+$	440, 498	0.001	2400	<0.02[g]
$[Ru(bpy)_2(dppzCN)]^{2+}$	681	0.002	8100	<0.02[h]
$[Ru(bpy)_2(dppzoxad)]^{2+}$	686	0.003	8200	0.08
$[Ir(dppzCN)(ppy)_2]^+$	676	0.002	6300	$\ll0.02$[f]
$[Ir(dppzoxad)(ppy)_2]^+$	668	0.006	6300	0.29

[a] λ_{PL} is the emission wavelength. [b] Φ_{PL} is the PL quantum yield determined using the reference compound $[Ru(bpy)_3]^{2+}$ and the method of Wang et al.[59] [c] Stokes shifts were obtained by taking the difference of the lowest energy absorption maximum and the emission maximum in wavenumbers. [d] τ is the excited-state lifetime. [e] As previously reported; included for comparison.[44] [f] No transient absorption or emission was observed. [g] Weak absorption at 370–420 nm could not be deconvoluted from the laser signal. [h] Absorption signal was too weak to be deconvoluted from the laser signal.

 © 2008 Wiley-VCH Verlag GmbH & Co. KGaA, Weinheim

$(dppzCN)(PPh_3)_2]^+$. The short excited-state lifetime of this complex is also consistent with allowed decay from a singlet excited state to a singlet ground state, as is the small Stokes shift. Phosphorescence in the Ru^{II} and Ir^{III} complexes appears to occur solely from ^{3}MLCT states. $[Ru(bpy)_2(dppzoxad)]^{2+}$ and $[Ir(dppzoxad)(ppy)_2]^+$ possess excited-state lifetimes in the usual range for Ru^{II} and Ir^{III} complexes, respectively.[41,53] The excited-state lifetimes for all of the complexes containing dppzCN are extremely short, which suggests that a rapid vibrational-decay pathway exists, presumably through vibration of the nitrile substituent. The quantum yields of the complexes are lower than what is usual for efficient OLED dopants. However, this may be offset by the good charge-transporting abilities of the materials to allow facile exciton formation.

Transient vibrational spectroscopy may be used to establish the nature of the excited states in polypyridyl complexes.[39,54–58] It is possible to probe the excited-state species with transient resonance Raman (TR^2) spectroscopy. By using a single-colour pump–probe protocol, excited-state transient Raman spectra were generated with 355 nm pulses. In the case of the ligands, such an experiment probes the ^{3}LC state. The transient resonance Raman spectra for dppzoxad and dppzCN differ markedly from the corresponding ground-state spectra. For dppzCN, strong ground-state features at 1341, 1349 and 1406 cm^{-1} are diminished in intensity and a new transient band at 1379 cm^{-1} grows in. Similarly, for dppzoxad the ground-state features at 1411, 1471 and 1540 cm^{-1} are much weaker in the transient spectrum and new bands are evident at 1380 and 1452 cm^{-1}, with the former band being very intense.

The spectrum of dppzCN* may be compared to the corresponding spectra of the complexes. In all cases the strong ^{3}LC marker band at 1380 cm^{-1} is evident (although it shifts to a slightly lower wavenumber); this strongly supports the assignment of the excited states in all three complexes (Cu, Re and Ru) to be LC in nature. In the case of the Cu and Re complexes there are also many ground-state bands present; this is consistent with the short lifetime of the transient state making it difficult to bleach the ground state in these experiments. Note that for $[Re(dppzCN)(CO)_3Cl]$ there are also transient bands at about 1357 cm^{-1} which may suggest some admixture of a secondary state. In the case of $[Re(dppzCN)(CO)_3Cl]$, spectroelectrochemical spectra reveal the signature for the $dppzCN^{\bullet-}$ species, which shows features at 1589 and 1270 cm^{-1} (resonant at 514.5 nm). The transient experiments are conducted at a different excitation wavelength, so the resonance effect for these bands will not be as strong, but there do not appear to be any radical-anion features present in the transient spectra; this suggests there is little MLCT state present under these conditions.

Conclusion

Dppz has been substituted at the 11-position with nitrile and 5-phenyl-1,3,4-oxadiazole moieties to produce ligands which were then coordinated to Re^I, Cu^I, Ru^{II} and Ir^{III} metal centres. In studying the structure, electrochemistry and spectroscopy of these systems, we find the following. 1) The dppz ligand is bent significantly in the crystal structures of $[Re(dppzCN)(CO)_3Cl]$ and $[Ru(bpy)_2(dppzoxad)]^{2+}$—calculations predict that the Re metal will lie out of ligand plane, but the observed phenomenon is greater than predicted. 2) The electronic structure suggests that the localised orbitals present in dppz are maintained in these ligands and their complexes. This is supported by resonance Raman spectroscopy, which shows that the ligand and metal-complex LC transitions are electronically equivalent. 3) The electrochemical behaviour of the complexes suggests that most form radical-anion species with reduction populating a phz-based SOMO—this is supported by the resonance Raman spectra of $[Re(dppzCN)(CO)_3Cl]^-$ and calculations on the reduced species. 4) Emission lifetimes were complicated by the interplay of these states and the presence of an efficient non-radiative pathway available to complexes of the nitrile ligand. The resonance Raman spectra of ligands and complexes both show ^{3}LC signatures, which suggests it is the dominant excited state formed with excitation. Quantum yields were lower than ideal for potential OLED dopants due to the low LUMO energy levels of the complexes. Prototype OLEDs containing these compounds have been investigated and the results of these studies will be reported shortly.

Experimental Section

Materials: 3,4-Diaminobenzonitrile was prepared from 4-aminobenzonitrile (Aldrich) via the intermediate 4-amino-3-nitrobenzonitrile by the methods of Kelly et al.[60] and Maruyama and Kawanishi.[61] 1,10-Phenanthroline-5,6-dione was synthesised from 1,10-phenanthroline by the method of Gillard et al.[62] Syntheses for 2-(11-dipyrido[3,2-*a*:2′,3′-*c*]phenazine)-5-phenyl-1,3,4-oxadiazole (dppzoxad) and *fac*-chlorotricarbonyl(2-(11-dipyrido[3,2-*a*:2′,3′-*c*]phenazine)-5-phenyl-1,3,4-oxadiazole)rhenium have been reported elsewhere.[44] Complexes of rhenium(I), copper(I), ruthenium(II) and iridium(III) containing the ligands were prepared by minor variations of reported literature procedures.[22,31,63] The precursors tetrakis(triphenylphosphine)copper tetrafluoroborate,[31] *cis*-bis(2,2′-bipyridine)dichlororuthenium[64] and tetrakis(2-phenylpyridine-C^2,N′)(μ-dichloro)diiridium[63] were prepared according to literature procedures.

11-Cyanodipyrido[3,2-*a*:2′,3′-*c*]phenazine (dppzCN): 4-Amino-3-nitrobenzonitrile (347 mg, 2.62 mmol) was added to a suspension of 1,10-phenanthroline-5,6-dione (460 mg, 2.19 mmol) in ethanol (60 mL) and the mixture was heated at reflux for 1 h. The solution was cooled, and the resulting precipitate was removed by filtration. The precipitate was dissolved in $CHCl_3$ and purified by column chromatography on neutral alumina with $CHCl_3$ as eluent. Yield 304 mg, 45%; ^{1}H NMR ($CDCl_3$, 300 MHz, 25°C): δ_H = 9.60 (td, 2H, J = 2.1, 8.4 Hz), 9.32 (dt, 2H, J = 2.1, 4.5 Hz), 8.73 (dd, 1H, J = 0.9, 1.8 Hz), 8.43 (dd, 1H, J = 0.9, 8.7 Hz), 8.03 (dd, 1H, J = 1.8, 8.7 Hz), 7.83 ppm (dd, 2H, J = 4.5, 8.4 Hz); ^{13}C NMR ($CDCl_3$, 300 MHz, 25°C): δ_C = 153.7, 153.5, 149.1, 148.8, 143.5, 143.0, 141.3, 135.9 (2C), 134.5, 134.3, 131.4 (2C), 130.9 (2C), 127.1, 124.6, 118.1, 114.1 ppm; MS (APCI POS): m/z 308 ($\{dppzCN+H\}^+$); elemental analysis calcd (%) for $C_{19}H_9N_5$: C 74.25, H 2.95, N 22.79; found: C 74.49, H 3.20, N 22.69.

***fac*-Chlorotricarbonyl(11-cyanodipyrido[3,2-*a*:2′,3′-*c*]phenazine)rhenium·0.5 H_2O ($[Re(dppzCN)(CO)_3Cl]\cdot 0.5\,H_2O$)**: Ethanol (50 mL) was purged with nitrogen for 5 min. Pentacarbonylchlororhenium(I) (144 mg,

 © 2008 Wiley-VCH Verlag GmbH & Co. KGaA, Weinheim

0.40 mmol) and dppzCN (123 mg, 0.40 mmol) were added, and the suspension was heated at reflux for 5 h under nitrogen and then cooled at −18 °C overnight. The resulting yellow precipitate was isolated by filtration, washed with diethyl ether (2×20 mL) and air-dried. Yield 159 mg, 65%; ^{1}H NMR ($CDCl_3$, 300 MHz, 25 °C): δ_H = 9.84 (ddd, 2H, J = 1.5, 5.1 Hz), 9.51 (dd, 2H, J = 1.5, 5.1 Hz), 8.75 (dd, 1H, J = 0.6, 1.8 Hz), 8.56 (dd, 1H, J = 0.6, 8.7 Hz), 8.17 (dd, 1H, J = 1.8, 8.7 Hz), 8.07 ppm (m, 2H); MS (APCI POS): m/z 308 ({dppzCN + H}$^+$), 578 ([Re(dppzCN)(CO)$_3$]$^+$); elemental analysis calcd (%) for $C_{22}H_{10}N_5O_{3.5}ClRe$: C 42.48, H 1.62, N 11.26, Cl 5.70; found: C 42.57, H 1.45, N 11.21, Cl 5.74.

Bis(triphenylphosphine)(11-cyanodipyrido[3,2-*a*:2′,3′-*c*]phenazine)copper(I) tetrafluoroborate ([Cu(dppzCN)(PPh$_3$)$_2$]$^+$): Diethyl ether (70 mL) was purged with nitrogen for 5 min. Tetrakis(triphenylphosphine)copper tetrafluoroborate (670 mg, 0.65 mmol) and dppzCN (200 mg, 0.65 mmol) were added and the suspension was stirred at room temperature under nitrogen for 48 h. The resulting yellow precipitate was isolate by filtration and then washed with diethyl ether (2×20 mL). The crude solid was recrystallised from the minimum volume of boiling methanol, to give a bright yellow powder. Yield 555 mg, 87%; ^{1}H NMR (300 MHz, $CDCl_3$, 25 °C): δ_H = 9.66 (m, 2H), 9.13 (m, 2H), 8.81 (d, 1H, J = 1.2 Hz), 8.50 (d, 1H, J = 8.7 Hz), 8.05 (dd, 1H, J = 1.8, 9.0 Hz), 7.91 (m, 2H), 7.51 (m, 6H), 7.34 ppm (m, 24H); MS (APCI POS): m/z 263 ({PPh$_3$ + H}$^+$), 308 ({dppzCN + H}$^+$); elemental analysis calcd (%) for $C_{55}H_{39}N_5P_2BF_4Cu$: C 67.25, H 4.00, N 7.13, P 6.31; found: C 66.93, H 4.01, N 7.07, P 6.26.

Bis(triphenylphosphine)(2-(11-dipyrido[3,2-*a*:2′,3′-*c*]phenazine)-5-phenyl-1,3,4-oxadiazole)copper(I) tetrafluoroborate·H$_2$O ([Cu(dppzoxad)(PPh$_3$)$_2$]$^+$): Diethyl ether (50 mL) was purged with nitrogen for 5 min. Tetrakis(triphenylphosphine)copper tetrafluoroborate (279 mg, 0.23 mmol) and dppzoxad (**1**; 100 mg, 0.23 mmol) were added and the suspension was stirred at room temperature under nitrogen for 48 h. The resulting yellow precipitate was isolated by filtration and then washed with diethyl ether (2×20 mL). The solid brown residue obtained was dissolved in CH_2Cl_2 and purified by column chromatography on neutral alumina with CH_2Cl_2 containing 2% methanol as eluent to give the product as a yellow powder. Yield 105 mg, 41%; ^{1}H NMR (300 MHz, $CDCl_3$, 25 °C): δ_H = 9.72 (m, 2H), 9.15 (s, 1H), 9.02 (m, 2H), 8.77 (d, 1H, J = 8.1 Hz), 8.55 (d, 1H, J = 9.3 Hz), 8.27 (m, 2H), 7.93 (m, 2H), 7.66 (m, 6H), 7.56 (m, 3H), 7.47 (m, 6H), 7.35 ppm (m, 18H); MS (ESI POS): m/z 587 ([Cu(PPh$_3$)$_2$]$^+$), 751 ([Cu(dppzoxad)(PPh$_3$)]$^+$); elemental analysis calcd (%) for $C_{62}H_{46}N_6P_2O_2BF_4Cu$: C 66.52, H 4.14, N 7.51, P 5.53; found: C 66.71, H 4.24, N 7.46, P 5.30.

Bis-2,2′-bipyridyl(11-cyanodipyrido[3,2-*a*:2′,3′-*c*]phenazine)ruthenium hexafluorophosphate·2H$_2$O ([Ru(bpy)$_2$(dppzCN)]$^{2+}$): *cis*-[Ru(bpy)$_2$Cl$_2$] (147 mg, 0.28 mmol) and dppzCN (121 mg, 0.39 mmol) were added to absolute ethanol (20 mL) and the suspension was heated at reflux overnight. The solvent was removed under reduced pressure with a rotary evaporator and the residue was then dissolved in H_2O (10 mL) and filtered through Celite to remove unreacted ligand. Saturated aqueous sodium hexafluorophosphate (2 mL) was added dropwise to the solution causing an orange precipitate to form. The precipitate was isolated by filtration, washed with ice-cold water (10 mL), 2-propanol (10 mL) and diethyl ether (30 mL) and then air-dried. The residue was dissolved in acetonitrile/saturated aqueous KNO_3 (7:1) solution and purified by column chromatography on silica gel with an acetonitrile/saturated aqueous KNO_3 (7:1) solution as the eluent. Metathesis of the complex to the hexafluorophosphate salt was achieved by dissolving the complex in the minimum volume of H_2O, addition of $NaPF_6$ and filtration of the resulting bright orange precipitate. Yield 221 mg, 64%; ^{1}H NMR (300 MHz, [D$_6$]DMSO, 25 °C): δ_H = 9.57 (m, 2H), 9.13 (d, 1H, J = 1.2 Hz), 8.89 (t, 4H, J = 8.1 Hz), 8.64 (d, 1H, J = 8.7 Hz), 8.41 (dd, 1H, J = 1.2, 8.7 Hz), 8.26 (m, 4H), 8.15 (t, 2H, J = 7.8 Hz), 8.05 (m, 2H), 7.80 (dd, 4H, J = 5.4, 13.5 Hz), 7.61 (t, 2H, J = 6.3 Hz), 7.40 ppm (t, 2H, J = 6.3 Hz); MS (ESI POS): m/z 360 ([Ru(bpy)$_2$(dppzCN)]$^{2+}$/2); elemental analysis calcd (%) for $C_{39}H_{29}N_9O_2F_{12}P_2Ru$: C 44.75, H 2.79, N 12.05; found: C 44.90, H 2.84, N 11.67.

Bis-2,2′-bipyridyl(2-(11-dipyrido[3,2-*a*:2′,3′-*c*]phenazine)-5-phenyl-1,3,4-oxadiazole)ruthenium triflate·H$_2$O ([Ru(bpy)$_2$(dppzoxad)]$^{2+}$): This complex was prepared in the same manner as [Ru(bpy)$_2$(dppzCN)]$^{2+}$ by using dppzoxad. The triflate salt of the complex was produced by addition of solid sodium triflate to an aqueous solution of the nitrate salt of the complex and isolation of the resulting orange precipitate by filtration. Yield 410 mg, 62%; ^{1}H NMR (300 MHz, [D$_6$]DMSO, 25 °C): δ_H = 9.66 (m, 2H), 9.23 (d, 1H, J = 1.8 Hz), 8.89 (t, 4H, J = 8.1 Hz), 8.83 (dd, 1H, J = 1.8, 9.0 Hz), 8.73 (d, 1H, J = 9.0 Hz), 8.28 (m, 4H), 8.22 (dd, 2H, J = 1.2, 8.4 Hz), 8.15 (m, 2H), 8.06 (m, 2H), 7.83 (d, 2H, J = 5.4 Hz), 7.79 (t, 2H, J = 4.2 Hz), 7.71 (m, 3H), 7.61 (t, 2H, J = 6.6 Hz), 7.41 ppm (t, 2H, J = 6.6 Hz); MS (ESI POS): m/z 420 ([Ru(bpy)$_2$(dppzoxad)]$^{2+}$/2); elemental analysis calcd (%) for $C_{48}H_{30}N_{10}O_7F_6S_2Ru$: C 50.66, H 2.66, N 12.31; found: C 50.36, H 2.71, N 12.12.

Bis(2-phenylpyridine-C^2,N′)(11-cyanodipyrido[3,2-*a*:2′,3′-*c*]phenazine)iridium hexafluorophosphate·2 ethyl acetate ([Ir(dppzCN)(ppy)$_2$]$^{2+}$): dppzCN (107 mg, 0.35 mmol) and tetrakis(2-phenylpyridine-C^2,N′)(μ-dichloro)diiridium (187 mg, 0.17 mmol) were added to methanol (40 mL) and the suspension was heated at reflux overnight. Saturated ammonium hexafluorophosphate in methanol (2 mL) was added dropwise to the cooled solution and the solvent was then removed under reduced pressure on a rotary evaporator. The residue was dissolved in CH_2Cl_2 and purified by column chromatography on SiO_2 with CH_2Cl_2/ethyl acetate (0 to 10% ethyl acetate) as eluent. The product was obtained as an orange solid following removal of solvent on a rotary evaporator. Yield 190 mg, 59%; ^{1}H NMR ($CDCl_3$, 300 MHz, 25 °C): δ_H = 9.80 (m, 2H), 8.77 (d, 1H, J = 1.2 Hz), 8.50 (m, 1H), 8.36 (d, 2H, J = 4.8 Hz), 8.05 (d, 1H, J = 8.7 Hz), 7.92 (m, 4H), 7.72 (m, 4H), 7.60 (t, 2H, J = 4.8 Hz), 7.09 (t, 2H, J = 7.5 Hz), 6.99 (t, 4H, J = 7.5 Hz), 6.40 ppm (d, 2H, J = 7.5 Hz); MS (APCI POS): m/z 308 ({dppzCN + H}$^+$), 501 ([Ir(ppy)$_2$]$^+$), 807 ([Ir(dppzCN)(ppy)$_2$]$^+$); elemental analysis calcd (%) for $C_{49}H_{41}N_7O_4PF_6Ir$: C 52.12, H 3.66, N 8.69; found: C 51.76, H 3.29, N 8.60.

Bis(2-phenylpyridine-C^2,N′)(2-(11-dipyrido[3,2-*a*:2′,3′-*c*]phenazine)-5-phenyl-1,3,4-oxadiazole)iridium hexafluorophosphate·ethanol ([Ir(dppzoxad)(ppy)$_2$]$^{2+}$): This complex was prepared in the same manner as [Ir(dppzCN)(ppy)$_2$]$^{2+}$ by using dppzoxad instead of dppzCN, and was obtained as an orange powder. Yield 174 mg, 62%; ^{1}H NMR ($CDCl_3$, 300 MHz, 25 °C): δ_H = 9.87 (m, 2H), 9.14 (d, 1H, J = 1.2 Hz), 8.76 (dd, 1H, J = 1.8, 9.0 Hz), 8.57 (d, 1H, J = 9.0 Hz), 8.37 (d, 2H, J = 4.5 Hz), 8.27 (m, 2H), 7.95 (m, 4H), 7.73 (m, 4H), 7.61 (m, 5H), 7.11 (t, 2H, J = 7.5 Hz), 7.02 (m, 4H), 6.41 ppm (d, 2H, J = 6.6 Hz); MS (ESI POS): m/z 925 ([Ir(dppzoxad)(ppy)$_2$]$^+$); elemental analysis calcd (%) for $C_{50}H_{36}N_8O_2PF_6Ir$: C 53.71, H 3.25, N 10.02; found: C 53.62, H 3.23, N 9.65.

Solid-state structures: Crystals of [Re(dppzCN)(CO)$_3$Cl] and [Ru(bpy)$_2$(dppzoxad)](CF$_3$SO$_3$)$_2$·2MeCN·H$_2$O were grown by slow evaporation from concentrated acetonitrile solutions. X-ray crystallographic data were collected at 85 K on a Bruker APEX II diffractometer with graphite monochromated $Mo_{K\alpha}$ radiation. Data were corrected for Lorentz and polarisation effects by using SAINT.[65] The structures were solved by direct methods with SIR-97[66] running within the WinGX v1.70.00 package,[67] with the resulting Fourier map revealing the location of all non-hydrogen atoms. Weighted full-matrix refinement on F^2 was carried out by using SHELXL-97[68] with all non-hydrogen atoms being refined anisotropically. Hydrogen atoms were included in the calculated positions and were refined as riding atoms with individual (or group, if appropriate) isotropic displacement parameters. Although the structure of [Re(dppzCN)(CO)$_3$Cl] refined well, there was found to be significant electron density within the cell that could not be reasonably assigned, and was thought to indicate the presence of one or more disordered solvent molecules. The SQUEEZE[69] option in PLATON was therefore used to investigate this possibility, as outlined in the CIF (see Supporting Information).

Instrumentation: ^{1}H and ^{13}C NMR spectra were obtained by using either a Varian VXR 300 MHz or Varian Europa 500 MHz spectrometer at room temperature. Chemical shift values are reported relative to residual solvent peaks. Elemental analyses were performed by the Campbell Microanalytical Laboratory, University of Otago. Mass spectrometry was performed on a Shimadzu QP8000 alpha spectrometer with an electrospray ionisation (ESI) or atmospheric pressure chemical ionisation

 © 2008 Wiley-VCH Verlag GmbH & Co. KGaA, Weinheim

(APCI) probe. Electronic spectra were recorded on a Varian Cary 500 Scan UV/Vis–near-infrared (NIR) spectrophotometer with Varian Cary Win UV Scan application v3.00 software. Solutions with a concentration of approximately 1×10^{-5} mol L^{-1} made up in spectroscopic-grade dichloromethane (or acetonitrile in the case of the Ru^{II} complexes) were used to perform absorption measurements. Emission spectra were recorded on a Perkin–Elmer luminescence spectrometer LS 50 B. Emission spectra were recorded from the same stock solutions as those used to record electronic absorption spectra. Tris(2,2′-bipyridyl)ruthenium(II) chloride hexahydrate was used as a standard for calculating quantum yields and was synthesised according to a literature procedure.[70] Cyclic voltammograms were recorded from nitrogen-purged 1 mM dichloromethane or acetonitrile solutions with 0.1 M tetrabutylammonium perchlorate as the supporting electrolyte. The electrochemical cell consisted of a 1-mm-diameter platinum working electrode embedded in a KeL-F cylinder with a platinum auxiliary electrode and a saturated potassium chloride calomel reference electrode. Potentials were recorded relative to the reference redox system of decamethylferrocenium/decamethylferrocene (−0.012 V in CH_2Cl_2 and 0.001 V in acetonitrile vs. Ag/AgCl/KCl (sat.))[71] and are reported relative to the saturated calomel electrode (SCE).[45] The potential of the cell was controlled by an EG&G PAR 273A potentiostat with model 270 software.

Excited-state measurements were performed at the University of Keele, England. Measurements were made on approximately 3×10^{-5} mol L^{-1} degassed solutions prepared in spectrophotometric-grade solvents at room temperature. Kinetic absorption and emission measurements employed the third harmonic (355 nm) of a Spectron Nd:YAG laser as the excitation source and a 250 W xenon arc lamp (Kratos) as the analysing source for the absorption measurements. The 355 nm beam was attenuated with neutral density filters such that the laser intensity at the sample was typically 20 mJ per pulse with a repetition rate of ≈1 Hz. The sample cell was a 10×10 mm^2 quartz cuvette fitted with a vacuum tap. An Applied Photophysics *f*/3.4 grating monochromator coupled to a Hamamatsu R928 photomultiplier tube was used. The transient absorption traces were fed to a Tektronix 2432A digital oscilloscope and the data transferred to an IBM-compatible PC through a GPIB interface. The limit of detection for these experiments was 20 ns.

Spectroelectrochemical measurements were performed using an optically transparent thin-layer electrode (OTTLE) cell.[72,73] Samples were made up in spectroscopic-grade dichloromethane or acetonitrile with a concentration of ≈0.5 mmol L^{-1} and contained 0.1 mol L^{-1} tetrabutylammonium perchlorate as the supporting electrolyte. Samples were deaerated by repeated freeze–pump–thaw cycles. The potential difference between the working and reference electrodes was controlled by an EG&G Model 174A polarographic analyser potentiostat. Spectra were obtained on a Varian Cary 500 Scan UV/Vis-NIR spectrophotometer with Varian Cary Win UV Scan application v3.00 software. An initial spectrum was recorded before the potentiostat was turned on, and then another was recorded with an applied potential of 0 V. The applied potential was then increased in 0.1 mV increments until a change in the absorption spectrum was observed. The applied potential was then held until changes in the absorption spectrum ceased, before increasing the applied potential in further 100 mV increments. The applied potential was then returned to 0 V to allow regeneration of the parent species and give a measure of the reversibility of the experiment. Difference spectra were obtained by subtracting the initial spectrum from subsequent measurements for each compound.

FTIR spectra of potassium bromide (KBr) disks were collected by using a Perkin–Elmer Spectrum BX FTIR system with Spectrum v.2.00 software. Spectra were measured for 64 scans with a resolution of 4 cm^{-1}. FT-Raman spectra were collected on powder samples by using a Bruker IFS-55 FT-interferometer bench equipped with an FRA/106 Raman accessory and utilising OPUS (version 4.0) software. A Nd:YAG laser with 1064 nm excitation wavelength was used. A liquid-nitrogen-cooled Ge diode (D418T) was used to detect Raman photons. Spectra were typically measured by using 16 scans at a power of 100 mW and a resolution of 4 cm^{-1}. Resonance Raman spectra were taken of 0.5 mM solutions of the ligand or complexes in $CDCl_3$ or MeCN. Solvents were obtained from Aldrich Chemicals. Resonance Raman spectra were generated with continuous-wave excitation by using a system previously described.[74,75] Spectra were analysed with GRAMS AI (Galactic Industries) and Origin 7.5 (OriginLab Corp) software.

Computational studies: The compounds were modelled by DFT (B3LYP) with a LANL2DZ effective core potential to describe the Re and Ru metals and a 6-31G(d) basis set for the other atoms. This was implemented by using the Gaussian 03W package.[76] To test if the calculated structures were reasonable models of the experimental data, frequency calculations were also conducted. The resulting calculated IR and Raman spectra were compared to experimental data. The mean absolute deviations for the calculated and experimental vibrational data were less than 10 cm^{-1} for each of the compounds. This level of agreement provided some confidence that the calculated properties were good models of the real system.[35,72] Calculations were also performed on the reduced complexes—for each of the species the spin expectation value, $<s^2>$, was approximately 0.7501. This is very close to that for a pure doublet.

Acknowledgement

We thank the MacDiarmid Institute for Advanced Materials and Nanotechnology for providing funding for this work.

[1] E. Holder, B. M. W. Langeveld, U. S. Schubert, *Adv. Mater.* **2005**, *17*, 1109–1121.
[2] M. Baldo, M. Segal, *Phys. Status Solidi A* **2004**, *201*, 1205–1214.
[3] G. Hughes, M. R. Bryce, *J. Mater. Chem.* **2005**, *15*, 94–107.
[4] J. Kido, Y. Okamoto, *Chem. Rev.* **2002**, *102*, 2357–2368.
[5] A. P. Kulkarni, C. J. Tonzola, A. Babel, S. A. Jenekhe, *Chem. Mater.* **2004**, *16*, 4556–4573.
[6] H. Yersin, *Top. Curr. Chem.* **2004**, *241*, 1–26.
[7] S. Fantacci, F. De Angelis, A. Sgamellotti, A. Marrone, N. Re, *J. Am. Chem. Soc.* **2005**, *127*, 14144–14145.
[8] C. Hiort, P. Lincoln, B. Norden, *J. Am. Chem. Soc.* **1993**, *115*, 3448–3454.
[9] E. R. Batista, R. L. Martin, *J. Phys. Chem. A* **2005**, *109*, 3128–3133.
[10] R. M. Hartshorn, J. K. Barton, *J. Am. Chem. Soc.* **1992**, *114*, 5919–5925.
[11] F. Westerlund, L. M. Wilhelmsson, B. Norden, P. Lincoln, *J. Phys. Chem. B* **2005**, *109*, 21140–21144.
[12] C. Turro, S. H. Bossmann, Y. Jenkins, J. K. Barton, N. J. Turro, *J. Am. Chem. Soc.* **1995**, *117*, 9026–9032.
[13] M. Cusumano, M. L. Di Pietro, A. Giannetto, *Inorg. Chem.* **2006**, *45*, 230–235.
[14] J. Fees, M. Ketterle, A. Klein, J. Fiedler, W. Kaim, *J. Chem. Soc. Dalton Trans.* **1999**, 2595–2600.
[15] B. J. Matthewson, A. Flood, M. I. J. Polson, C. Armstrong, D. L. Phillips, K. C. Gordon, *Bull. Chem. Soc. Jpn.* **2002**, *75*, 933–942.
[16] M. R. Waterland, K. C. Gordon, *J. Raman Spectrosc.* **2000**, *31*, 243–253.
[17] J. Fees, W. Kaim, M. Moscherosch, W. Matheis, J. Klima, M. Krejcik, S. Zalis, *Inorg. Chem.* **1993**, *32*, 166–174.
[18] D. P. Rillema, D. S. Jones, C. Woods, H. A. Levy, *Inorg. Chem.* **1992**, *31*, 2935–2938.
[19] S. F. Haddad, J. A. Marshall, G. Crosby, B. Twamley, *Acta Crystallogr. Sect. E: Struct. Rep. Online* **2002**, *58*, 559–561.
[20] M. I. J. Polson, S. L. Howell, A. H. Flood, A. K. Burrell, A. G. Blackman, K. C. Gordon, *Polyhedron* **2004**, *23*, 1427–1439.
[21] J. Rusanova, S. Decurtins, E. Rusanov, H. Stoeckli-Evans, S. Delahaye, A. Hauser, *J. Chem. Soc. Dalton Trans.* **2002**, 4318–4320.
[22] N. J. Lundin, P. J. Walsh, S. L. Howell, J. J. McGarvey, A. G. Blackman, K. C. Gordon, *Inorg. Chem.* **2005**, *44*, 3551–3560.
[23] S. Dhar, P. A. N. Reddy, M. Nethaji, S. Mahadevan, M. K. Saha, A. R. Chakravarty, *Inorg. Chem.* **2002**, *41*, 3469–3476.

 © 2008 Wiley-VCH Verlag GmbH & Co. KGaA, Weinheim

[24] M. Kato, C. Kosuge, S. Yano, M. Kimura, *Acta Crystallogr. Sect. C: Cryst. Struct. Commun.* **1998**, *54*, 621–623.
[25] V. W.-W. V. Yam, K. K.-W. Lo, K.-K. Cheung, R. Y.-C. Kong, *J. Chem. Soc. Dalton Trans.* **1997**, 2067–2072.
[26] V. W.-W. Yam, K. K.-W. Lo, K.-K. Cheung, R. Y.-C. Kong, *J. Chem. Soc. Chem. Commun.* **1995**, 1191–1193.
[27] T. Phillips, I. Haq, A. J. H. M. Meijer, H. Adams, I. Soutar, L. Swanson, M. J. Sykes, J. A. Thomas, *Biochemistry* **2004**, *43*, 13657–13665.
[28] C. Janiak, *J. Chem. Soc. Dalton Trans.* **2000**, 3885–3896.
[29] F. De Angelis, S. Fantacci, A. Selloni, *Chem. Phys. Lett.* **2004**, *389*, 204–208.
[30] To account for the great variation in MO energy levels calculated for the different compounds, we have calibrated the energy levels to the $1b_1$ ligand MO for each of the systems. This MO has no amplitude at the chelating N atoms or at the 11-position.
[31] M. R. Waterland, K. C. Gordon, J. J. McGarvey, P. M. Jayaweera, *J. Chem. Soc. Dalton Trans.* **1998**, 609–616.
[32] R. J. H. Clark, T. J. Dines, *Angew. Chem.* **1986**, *98*, 131–160; *Angew. Chem. Int. Ed.* **1986**, *25*, 131–158.
[33] A. Y. Hirakawa, M. Tsuboi, *Science* **1975**, *188*, 359–361.
[34] M. R. Waterland, S. L. Howell, K. C. Gordon, A. K. Burrell, *J. Phys. Chem. A* **2005**, *109*, 8826–8833.
[35] S. L. Howell, K. C. Gordon, *J. Phys. Chem. A* **2006**, *110*, 4880–4887.
[36] J. C. Earles, K. C. Gordon, D. L. Officer, P. Wagner, *J. Phys. Chem. A* **2007**, *111*, 7171–7180.
[37] H. D. Stoeffler, N. B. Thornton, S. L. Temkin, K. S. Schanze, *J. Am. Chem. Soc.* **1995**, *117*, 7119–7128.
[38] J. Dyer, W. J. Blau, C. G. Coates, C. M. Creely, J. D. Gavey, M. W. George, D. C. Grills, S. Hudson, J. M. Kelly, P. Matousek, J. J. McGarvey, J. McMaster, A. W. Parker, M. Towrie, J. A. Weinstein, *Photochem. Photobiol. Sci.* **2003**, *2*, 542–554.
[39] S. L. Howell, K. C. Gordon, J. J. McGarvey, *J. Phys. Chem. A* **2005**, *109*, 2948–2956.
[40] Y. Li, Y. Cao, J. Gao, D. Wang, G. Yu, A. J. Heeger, *Synth. Met.* **1999**, *99*, 243–248.
[41] K. K.-W. Lo, C.-K. Chung, N. Zhu, *Chem. Eur. J.* **2006**, *12*, 1500–1512.
[42] K. K.-W. Lo, D. C.-M. Ng, C.-K. Chung, *Organometallics* **2001**, *20*, 4999–5001.
[43] E. Amouyal, A. Homsi, J. C. Chambron, J. P. Sauvage, *J. Chem. Soc. Dalton Trans.* **1990**, 1841–1845.
[44] N. J. Lundin, A. G. Blackman, D. L. Officer, K. C. Gordon, *Angew. Chem.* **2006**, *118*, 2644–2646; *Angew. Chem. Int. Ed.* **2006**, *45*, 2582–2584.
[45] A. J. Bard, L. R. Faulkner, *Electrochemical Methods*, Wiley, New York, **2001**, p. 833.
[46] G. David, P. J. Walsh, K. C. Gordon, *Chem. Phys. Lett.* **2004**, *383*, 292–296.
[47] D. G. Cuttell, S.-M. Kuang, P. E. Fanwick, D. R. McMillin, R. A. Walton, *J. Am. Chem. Soc.* **2002**, *124*, 6–7.
[48] S. M. Scott, K. C. Gordon, A. K. Burrell, *Inorg. Chem.* **1996**, *35*, 2452–2457.
[49] S. E. Page, K. C. Gordon, A. K. Burrell, *Inorg. Chem.* **1998**, *37*, 4452–4459.
[50] M. R. Waterland, T. J. Simpson, K. C. Gordon, A. K. Burrell, *J. Chem. Soc. Dalton Trans.* **1998**, 185–192.
[51] M. S. Lowry, W. R. Hudson, R. A. Pascal, Jr., S. Bernhard, *J. Am. Chem. Soc.* **2004**, *126*, 14129–14135.
[52] D. J. Casadonte, D. R. McMillin, *J. Am. Chem. Soc.* **1987**, *109*, 331–337.
[53] N. Komatsuzaki, R. Katoh, Y. Himeda, H. Sugihara, H. Arakawa, K. Kasuga, *J. Chem. Soc. Dalton Trans.* **2000**, 3053–3054.
[54] M. W. George, J. J. Turner, *Coord. Chem. Rev.* **1998**, *177*, 201–217.
[55] P. J. Walsh, K. C. Gordon, N. J. Lundin, A. G. Blackman, *J. Phys. Chem. A* **2005**, *109*, 5933–5942.
[56] P. Chen, K. M. Omberg, D. A. Kavaliunas, J. A. Treadway, R. A. Palmer, T. J. Meyer, *Inorg. Chem.* **1997**, *36*, 954–955.
[57] C. G. Coates, J. Olofsson, M. Coletti, J. J. McGarvey, B. Oenfelt, P. Lincoln, B. Norden, E. Tuite, P. Matousek, A. W. Parker, *J. Phys. Chem. B* **2001**, *105*, 12653–12664.
[58] M. K. Kuimova, D. C. Grills, P. Matousek, A. W. Parker, X.-Z. Sun, M. Towrie, M. W. George, *Vib. Spectrosc.* **2004**, *35*, 219–223.
[59] K. Wang, L. Huang, L. Gao, L. Jin, C. Huang, *Inorg. Chem.* **2002**, *41*, 3353–3358.
[60] D. P. Kelly, S. A. Bateman, R. F. Martin, M. E. Reum, M. Rose, A. R. D. Whittaker, *Aust. J. Chem.* **1994**, *47*, 247–262.
[61] S. Maruyama, Y. Kawanishi, *J. Mater. Chem.* **2002**, *12*, 2245–2249.
[62] R. D. Gillard, R. E. E. Hill, R. Maskill, *J. Chem. Soc. A* **1970**, 1447–1451.
[63] V. Marin, E. Holder, R. Hoogenboom, U. S. Schubert, *J. Polym. Sci. Part A: Polym. Chem.* **2004**, *42*, 4153–4160.
[64] M. E. Marmion, K. J. Takeuchi, *J. Am. Chem. Soc.* **1988**, *110*, 1472–1480.
[65] I. Siemens Analytical X-ray Systems in SAINT, Madison, WI, **1996**.
[66] A. Altomere, M. C. Burla, M. Camilla, G. L. Cascarano, C. Giacovazzo, A. Guagliardi, A. G. G. Moliterni, G. Polidori, R. Spagna, *J. Appl. Crystallogr.* **1999**, *32*, 115.
[67] L. J. Farrugia, *J. Appl. Crystallogr.* **1999**, *32*, 837.
[68] G. M. Sheldrick in *SHELXL-97*, Program for the Refinement of Crystal Structures, University of Göttingen, **1997**.
[69] P. van der Sluis, A. L. Spek, *Acta Crystallogr. A* **1990**, *46*, 194–201.
[70] J. A. Broomhead, C. G. Young, *Inorg. Synth.* **1990**, *28*, 338–340.
[71] I. Noviandri, K. N. Brown, D. S. Fleming, P. T. Gulyas, P. A. Lay, A. F. Masters, L. Phillips, *J. Phys. Chem. B* **1999**, *103*, 6713–6722.
[72] S. L. Howell, B. J. Matthewson, M. I. J. Polson, A. K. Burrell, K. C. Gordon, *Inorg. Chem.* **2004**, *43*, 2876–2887.
[73] J. Sherborne, S. M. Scott, K. C. Gordon, *Inorg. Chim. Acta* **1997**, *260*, 199–205.
[74] T. M. Clarke, K. C. Gordon, D. L. Officer, D. K. Grant, *J. Chem. Phys.* **2006**, *124*, 164501.
[75] P. J. Walsh, K. C. Gordon, P. Wagner, D. L. Officer, *ChemPhysChem* **2006**, *7*, 2358–2365.
[76] Gaussian 03W, M. J. Frisch, G. W. Trucks, H. B. Schlegel, G. E. Scuseria, M. A. Robb, J. R. Cheeseman, J. A. Montgomery, Jr., T. Vreven, K. N. Kudin, J. C. Burant, J. M. Millam, S. S. Iyengar, J. Tomasi, V. Barone, B. Mennucci, M. Cossi, G. Scalmani, N. Rega, G. A. Petersson, H. Nakatsuji, M. Hada, M. Ehara, K. Toyota, R. Fukuda, J. Hasegawa, M. Ishida, T. Nakajima, Y. Honda, O. Kitao, H. Nakai, M. Klene, X. Li, J. E. Knox, H. P. Hratchian, J. B. Cross, C. Adamo, J. Jaramillo, R. Gomperts, R. E. Stratmann, O. Yazyev, A. J. Austin, R. Cammi, C. Pomelli, J. W. Ochterski, P. Y. Ayala, K. Morokuma, G. A. Voth, P. Salvador, J. J. Dannenberg, V. G. Zakrzewski, S. Dapprich, A. D. Daniels, M. C. Strain, O. Farkas, D. K. Malick, A. D. Rabuck, K. Raghavachari, J. B. Foresman, J. V. Ortiz, Q. Cui, A. G. Baboul, S. Clifford, J. Cioslowski, B. B. Stefanov, G. Liu, A. Liashenko, P. Piskorz, I. Komaromi, R. L. Martin, D. J. Fox, T. Keith, M. A. Al-Laham, C. Y. Peng, A. Nanayakkara, M. Challacombe, P. M. W. Gill, B. Johnson, W. Chen, M. W. Wong, C. Gonzalez, J. A. Pople, Gaussian, Inc., Pittsburgh, PA, **2003**.

Received: July 7, 2008
Revised: August 30, 0000
Published online: November 19, 2008

 © 2008 Wiley-VCH Verlag GmbH & Co. KGaA, Weinheim